Comparison of transport methodologies on near-field pollutant dispersion in urban environments using CFD

†*Clarence TEE[1], E.Y.K. NG[1] and George XU[2]

[1]School of Mechanical & Aerospace Engineering, Nanyang Technological University, Singapore.
[2]Fluid Dynamics Department, Institute of High-Performance Computing, A*STAR, Singapore.
†Corresponding author: clarenceteee@gmail.com

Abstract

Until recently, the use of Computational Fluid Dynamics (CFD) appears to be gaining traction over traditional Gaussian Dispersion Modeling to predict and understand pollutant dispersion processes in urban environments. Gaussian Dispersion Models, while computationally fast, lacks in physical representation and accuracy but still sufficed as evidenced by its use in numerous engineering designs and research applications. In CFD, two typical methodologies namely the passive scalar transport and the multi-species transport are used to track spatial dispersion of pollutants. The focus of this study is to understand and quantify the differences between the two models when applied to near-field dispersion of heavy gases. The two methodologies are validated by simulating the dispersion phenomena for two test cases which largely bears resemblance to urban settings: a three-dimensional street canyon setup and the Mock Urban Setting Test (MUST) field experiment. The pollutant used in the CODASC study is Sulphur Hexafluoride (SF_6) while Propylene (C_3H_6) is used in MUST, both heavier than air. It is found that numerical results are highly sensitive to the value of turbulent Schmidt number (Sc_t) in both test cases. Through parametric studies, the best accuracy is attained when the Sc_t value of 0.5 is used in the street canyon case and Sc_t value of 1.5 for MUST. Generally, better agreement between numerical and experimental results is reflected in the street canyon case study compared to MUST. For the CODASC case study, the passive scalar transport model yielded better results than the multi-species transport model while the opposite is true for MUST. With the preconceived notion that the multi-species transport model should outperform the passive scalar transport, a conclusion showing a lack of significant improvement the former has over the passive scalar transport model is indeed unexpected. With regards to computational efficiency, the passive scalar transport model requires much lesser resources such as CPU time and memory compared to the multi-species transport model, thus making it more efficient.

Keywords: CFD, pollutant dispersion, near-field, urban environment modeling, turbulence modeling

Introduction

Pollutant dispersion modeling holds significant importance when determining the severity of disasters, be it natural or man-made. Incidents such as the Fukushima Daiichi accident in 2011 or the more recent 2018 gas leak in Zhangjiakou, China have shown the devastating consequences on air quality through the release of toxic materials into the atmosphere. Even eight years after the disaster, atmospheric air quality around the immediate vicinity of Fukushima still contains lethal levels of radiation [1] and the effects of the incident in Zhangjiakou led to tragic consequences, due to the dispersion of a flammable pollutant which was ignited, leading to fatalities [2]. It is therefore of paramount importance to understand and assess these effects on public health and safety, immediately following an accident or to conduct risk management planning for pre-emptive purposes. The importance of understanding atmospheric dispersion processes is further emphasized through the span of research in developing state-of-the-art models from regulatory bodies such as the United States Environmental Protection Agency (US EPA) and UK Met Office to research organizations such as the European Cooperation in Science & Technology (COST). Many of these regulatory

bodies have developed their own atmospheric dispersion models: for instance, the open-source AERMOD was developed by US EPA and NAME by the UK Met Office [3]. In general, dispersion models are classified into three different families of models: Gaussian, Lagrangian and Eulerian. These models have been used to good effect in disasters such as the Eyjafjallajökull eruption and the Fukushima nuclear accident to provide crucial information for timely and preventive measures. Private research organizations have also funded initiatives to understand and improve the quality of models used to predict transport phenomena such as the COST Action 732.

However, effectiveness and reliability of these dispersion models are confined to certain spatial scales namely the meteorological mesoscale which would not be suitable for analyzing dispersion in the urban environment, the scale of which is two orders of magnitude smaller than meteorological mesoscale. Hence Lagrangian and Eulerian models will not work well for modeling dispersion on a microscale level. Gaussian-based models do have its merits when used on that spatial scale but the interaction between complex flow fields and different building configurations limit its accuracy significantly. Besides Gaussian-based models, microscale Computational Fluid Dynamics (CFD) are commonly used. The cost involving CFD simulations is relatively low, detailed information about the flow field can be obtained depending on mesh resolution and scaling of simulations can be carried out with ease [4]. But since errors are introduced in each progressive stage of CFD modeling, accuracy and reliability of results are often questioned which require validation studies.

Gaussian Dispersion Modeling

The underlying equation of Gaussian-based models is given by:

$$c(x,y,z) = \frac{Q}{2\pi\sigma_y\sigma_z u}\exp\left(-\frac{y^2}{2\sigma_y^2}\right)\left(\exp\left(-\frac{(z-H_e)^2}{2\sigma_z^2}\right)+\exp\left(-\frac{(z+H_e)^2}{2\sigma_z^2}\right)\right) \quad (1)$$

where c is the concentration of a pollutant at a given location, Q is the rate of pollutant emission, H_e is the effective height of release which is the sum of actual stack height H_p and plume rise Δh, u is the speed of wind in the x-direction at height H_e. σ_y and σ_z are standard deviations of the pollutant concentration profile in the y and z direction respectively, both represented by a Gaussian distribution which depends heavily on atmospheric turbulence. Comprehensive experimental measurements have been carried out to relate various values of σ to atmospheric stability. The resulting tabulated data is known as the Pasquill-Gifford-Turner Stability Classifications [5]. Stratification of the atmosphere into different stability classes is crucial to model the atmospheric boundary layer accurately. The boundary layers are differentiated into three main types: unstable, neutral and stable.

The popularity of Gaussian models is largely due to its low computational costs, with many environmental regulatory agencies using it as an initial assessment in determining the severity of industrial accidents or pollution levels. Complex dispersion related phenomena can be included which adds an edge of versatility to Gaussian models. However, its validity and accuracy are dampened by underlying assumptions used in the derivation of Eq. (1). Velocities in the y and z direction are assumed to be zero and diffusion in the x direction is ignored. Neglecting diffusion in the x direction can lead to inaccurate results especially in situations where there are low wind speeds which causes significant concern. Atmospheric turbulence is also assumed to be uniform and homogenous since σ is directly proportional to sizes of eddies. Furthermore, σ values are measured from rural terrains with flat and open surfaces, which reduce its applicability when the model is used in an urban environment [6, 7]. A sensitivity study on the parameters of the Gaussian model by Adel [6] showed that changes as small as

10% could result in 100% under or over prediction. Hence using Gaussian models for dispersion in urban environments raises questionable issues in accuracy and applicability.

Within urban environments, buildings and obstacles as well as their complex interaction with flow fields bring additional challenges in dispersion modeling. Near-field dispersion is characterized by interactions between atmospheric boundary layer flows and flow structures around buildings while in far-field dispersion, the horizontal motion proves to be more dominant over vertical motions and effects of buildings on flow fields are limited [8]. More specifically in near-field dispersion, there are features such as a fully three-dimensional flow structure around buildings which affects pollutant transport in ways that could not be fully described by Gaussian models. Flow separation, recirculation and various patterns of vortices (e.g. horseshoe vortices, vortex shedding etc.) generated by the presence of buildings adds further complication in determining pollutant distribution at the desired location.

Computational Fluid Dynamics (CFD)

Interest in CFD to model pollutant dispersion in urban environments is not newly found as seen by the review of Tominaga and Stathopoulos [8], which offered a comprehensive compilation of current modeling techniques. The use of CFD has allowed the approximation of flow field quantities such as velocities and concentration to be made known throughout the computational domain in all three-dimensions, which Gaussian-based models lack. However, CFD is not without uncertainties. The validation and verification of CFD models constitute a major role in forming a quantitative conclusion on the accuracy and the reliability of results. Availability of experimental data while reassuring, is to be used with caution as circumstances surrounding the experiment must be replicated in the CFD model through initial and boundary conditions, failing which will render the comparison between numerical and experimental data pointless [8]. Inherent in such a strict requirement is the assumption that every experiment must be carried out under identical conditions. This hints at some form of replicability which is mostly impossible when meteorological factors like wind and weather conditions are involved [9]. Even under more predictable conditions such as wind tunnel testing, drawbacks still exist, nonetheless. Therefore, a certain pre-existing error must be accepted into the overall model evaluation.

The motivation behind this study is largely due to limited efforts thus far to compare the differences between passive scalar transport and multi-species transport. With the passive scalar transport model, the concentration of pollutant does not have any impact on the flow field. As such, flow properties remain unchanged even if a different pollutant is used. The pollutant used can be interpreted to be weightless and its transport is mainly governed by advection and mass diffusion. Using the multi-species transport model, on the other hand, will result in the flow field changing depending on the chemical species being transported. Since the mixing law takes effect, any change in composition in the mixture of species will affect the density of the resulting mixture. Gravitational effects are also included where physical characteristics of the pollutant will affect the flow field. The two species considered in this study will be the pollutant and air. Chemical reactions between the two species are however, ignored in this study.

A review by Lateb et al. [4] on CFD to predict dispersion in urban environments stated that a common assumption used by various studies is that the pollutants are assumed to be passive and subsequently, the effects physical characteristics of pollutant particles have on the flow field are often neglected. A study previously done by Gromke and Ruck [11] [12] investigated pollutant dispersion in a three-dimensional tree free street canyon and found that concentration values predicted by FLUENT gave good agreement to wind tunnel measurements. Species transport was utilized but they did not study the effects of a passive pollutant. Bekka et al. [13]

carried out a study based on the MUST case and found that agreement with full-scale experimental data [14] varied with distance from the source. Better agreement was observed closer to the source while more deviation was observed further from the source but there was no indication on how transport of the pollutant was modeled, raising some doubt over the quality of their findings. Tominaga and Stathopoulos [15] carried out a comparison between neutrally buoyant (passive) scalars and heavy gases on flow and concentration fields and found that prediction performance of heavy gases was worse than that for neutral gases, but their scope was limited to just one building configuration.

Objective

The objective of this study is to present and evaluate CFD methods for the dispersion of heavy gases in urban environments using the commercial code FLUENT. Two different methodologies: 1) passive scalar transport and 2) multi-species are proposed to track dispersion of pollutant particles. The two methodologies are validated through two test cases representative of urban environments: a three-dimensional street canyon and the Mock Urban Setting Test (MUST). First, the respective mathematical models are analysed. Following that, the characteristics of both case studies used for validation purposes are identified. Besides visual observation and comparison of numerical results with experimental data, statistical performance measures are subsequently introduced to provide a succinct approach in quantifying the performance of each methodology. Results and discussion of the two methodologies are subsequently given, where the effects Sc_t values have on concentration distributions are discussed. A comparison between both methodologies is rendered and their accuracy is evaluated.

Fundamental Mathematical Models

The Standard Gradient Diffusion Hypothesis (SGDH) is primarily used to model the turbulent scalar fluxes, which are postulated to be directly proportional to concentration gradients with a coefficient of proportionality known as turbulent diffusivity, D_t:

$$u'c' = D_t \frac{\partial \bar{c}}{\partial x} \tag{2}$$

$$v'c' = D_t \frac{\partial \bar{c}}{\partial y} \tag{3}$$

$$w'c' = D_t \frac{\partial \bar{c}}{\partial z} \tag{4}$$

Turbulent diffusivity can be further broken down into a ratio of two terms: turbulent kinematic viscosity (ν_t) over the turbulent Schmidt number (Sc_t). It should be noted that Sc_t is a free parameter, with multiple ranges of values that depend on flow fields and configurations of geometries with which the flow interacts with. This seems to suggest that Sc_t can be altered to artificially increase or reduce turbulent diffusion which can drastically affect transport phenomena and subsequently, numerically predicted concentration.

Tominaga and Stathopoulos [17] showed that Sc_t ranged from 0.2 to 1.3 which differed from the commonly used values of 0.7 to 0.9. Gualtieri et al. [18] discovered in his analysis of literature from both water and atmospheric systems that the range of best-fitting Sc_t changes for different cases and that there were cases where best-fit Sc_t value was found to be the same for extremely different flow conditions (i.e. cases of water and atmospheric systems having similar Sc_t values). These two inconsistent observations contributed to a conclusion that it is impossible to determine a generic Sc_t value. Gualtieri et al. subsequently questioned if Sc_t had

different values in the same flow domain but was inconclusive as to which parameters controlled this variability.

The relevant governing equations begin with the continuity equation:

$$\nabla \cdot (\rho \vec{v}) = 0 \tag{5}$$

Reynolds Averaged Navier-Stokes, also known as the momentum equations:

$$\rho(\vec{v} \cdot \nabla u) = -\frac{\partial p}{\partial x} + (\mu + \mu_t)\nabla \cdot (\nabla u) \tag{6}$$

$$\rho(\vec{v} \cdot \nabla v) = -\frac{\partial p}{\partial y} + (\mu + \mu_t)\nabla \cdot (\nabla v) \tag{7}$$

$$\rho(\vec{v} \cdot \nabla w) = -\frac{\partial p}{\partial z} + (\mu + \mu_t)\nabla \cdot (\nabla w) \tag{8}$$

k-ϵ turbulence model:

$$\nabla \cdot (\rho \vec{v} k) = \nabla \cdot \left(\mu + \frac{\mu_t}{\sigma_k}\nabla k\right) + P_k - \rho\varepsilon \tag{9}$$

$$\nabla \cdot (\rho \vec{v} \varepsilon) = \nabla \cdot \left(\mu + \frac{\mu_t}{\sigma_\varepsilon}\nabla \varepsilon\right) + C_{\varepsilon 1} P_k \frac{\varepsilon}{k} - C_{\varepsilon 2}\rho \frac{\varepsilon^2}{k} \tag{10}$$

$$\mu_t = \rho C_\mu \frac{k^2}{\varepsilon} \tag{11}$$

$$P_k = \mu_t (\nabla \vec{v})^2 \tag{12}$$

Passive scalar transport equation:

$$\nabla \cdot (\vec{v} c) = \nabla \cdot \left[\left(D_c + \frac{\nu_t}{Sc_t}\right)\nabla c\right] + S_c \tag{13}$$

where c is the concentration of the scalar, D_c is laminar diffusivity and S_c is the source term. The multi-species transport model also utilizes Eqns. (5) to (12) but continues to Eqn. (14) and (15):

$$\nabla \cdot (\rho Y_i \vec{v}) = -\nabla \cdot J_i + S_i \tag{14}$$

$$J_i = -\left(\rho D_i + \frac{\mu_t}{Sc_t}\right)\nabla Y_i \tag{15}$$

where S_i is the source term for the i^{th} species, J_i is the diffusion flux of species i which is due to concentration gradients, D_i is the mass diffusion coefficient for species i in the mixture and Y_i is the mass fraction of species i. Eq. (14) and Eq. (15) solve for the mass fraction, Y_i as each constituent of the mixture is represented with $i = 1, 2$ …etc.

Case Studies

CODASC

As part of a larger effort in air quality studies to quantify the effects of tree planting on dispersion of traffic emissions by the Karlsruhe Institute of Technology (KIT), a database named Concentration Data of Street Canyons (CODASC) was established from the results of wind tunnel experiments with varying parameters and street canyon/tree avenue configurations

[20]. For the scope of this study, it suffices to consider only a tree-free street canyon configuration in three dimensions. The street canyon model is scaled down to 1:150, with $L = 180\ m$, $H = W = 18\ m$. Four lines of tracer pollutant release, with the intention of emulating traffic exhaust, are placed in between the two building blocks and it exceeds the street canyon by about 10% on each side to consider pollutant release from traffic junctions. SF_6 was used as a pollutant in this case and the release is distributed through equally spaced perforations. Dimensions of computational domain and the street canyon are shown in Fig. 1. Experimental data for various scenarios was made available through the online database [20].

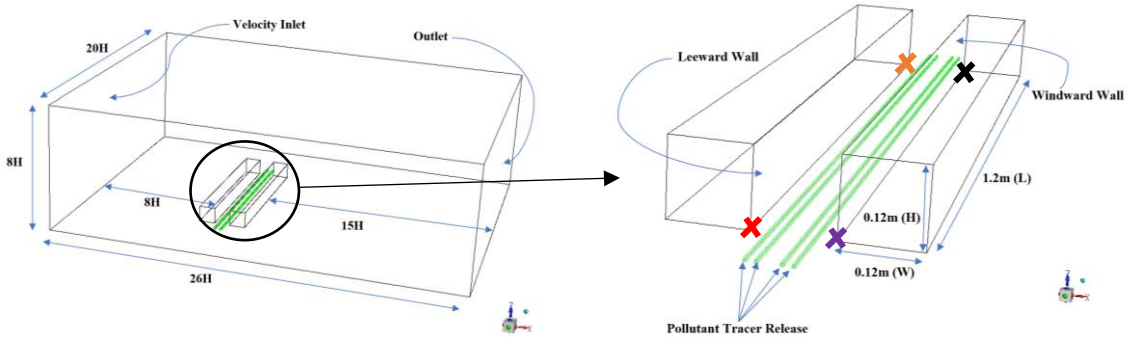

Figure 1. *Dimensions of CODASC street canyon model.*

Inlet wind velocity is in the x-direction, perpendicular to the building blocks and it follows a power law profile in a neutrally stratified atmospheric boundary layer:

$$\frac{u(z)}{u(z_{ref})} = \left(\frac{z}{z_{ref}}\right)^{\alpha} \tag{16}$$

z_{ref} is the reference height which is 0.12 m and the flow velocity at the reference height, $u(z_{ref})$ is 4.70 m/s. Similarly, $u(z)$ is the velocity at a given height z. α is the wind shear exponent of 0.3. k and ϵ profiles are specified as follows:

$$k = \frac{u_*^2}{\sqrt{C_\mu}}\left(1 - \frac{z}{\delta}\right) \tag{17}$$

$$\varepsilon = \frac{u_*^3}{\kappa z}\left(1 - \frac{z}{\delta}\right) \tag{18}$$

where u_* is the friction velocity of 0.52 m/s and C_μ is 0.09 which is the turbulence model constant. δ is the boundary layer thickness, κ is von Kármán's constant and both have values of 0.96 and 0.4 respectively. The variable of interest is the non-dimensional concentration value c^+ which is normalized:

$$c^+ = \frac{cu_H H}{Q/l} \tag{19}$$

where c is the measured concentration, u_H is equivalent to $u(z_{ref})$ and Q/l is the tracer source strength of SF_6 per unit length. The main point of interest is the normalized concentration distribution of the leeward and windward side of the street canyon.

Mock Urban Setting Test (MUST)

MUST is a full-scale, outdoor experiment free from laboratory limitations conducted at the U.S. Army Dugway Proving Ground (DPG) Horizontal Grid test site [14]. Motivation for MUST primarily grew out of a need for field data to be obtained outside laboratory conditions for the

verification and validation of models developed to understand dispersion mechanisms and the full effects of atmospheric boundary layers and surface roughness on transport phenomena in an urban setting. The setup configuration of MUST comprises of shipping containers each 12.2 m long, 2.42 m wide and 2.54 m high arranged in a 12 by 10 array in a 200 m squared area. With reference to the original report [14], trial name #2681829 is selected to be replicated in this present study by means of numerical methods. Propylene (C_3H_6) is used as a tracer gas and is released at a height of 1.8 m above ground at a rate of 225 litres per minute and the location of release is marked by a cross in Fig. 2. 48 sensors were strategically placed at areas of interest to measure concentrations; 40 of which are distributed evenly across the array at a height of 1.6 m above ground and are denoted by the orange points. The other 8 are placed 1, 2, 4, 6, 8, 10, 12 and 16 m above ground level at a single location in the middle of the array, where the green point is. The dimensions of the computational domain are shown in Fig. 3.

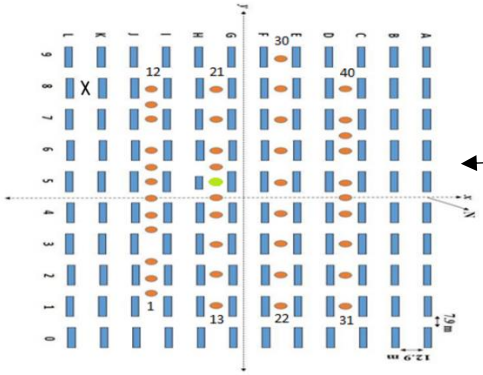

Figure 2. *Layout of test case #2681829 and locations of sensors 1 to 48 (Image taken from [12]).*

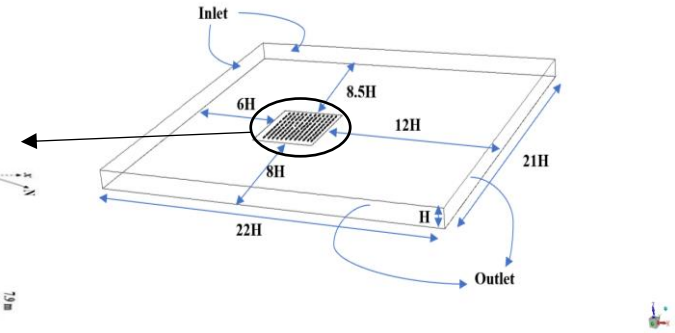

Figure 3. *Dimensions of computational domain for MUST.*

Given the nature of MUST experiments (i.e. outdoor and full-scale), it is necessary to model the atmospheric boundary layer (ABL) to obtain accurate and reliable predictions of atmospheric-related phenomena [21]. More specifically, the modeled ABL must be horizontally homogenous which is achieved when inlet profiles of mean wind speed and turbulence quantities are in equilibrium with the wall functions used. With a horizontally homogenous ABL, streamwise gradients will be prevented from forming in these profiles as the flow progresses to simulate the phenomena of interest. This study focuses on a neutrally stratified ABL since thermal and buoyancy effects on turbulence are not considered. The most commonly used boundary conditions to simulate the ABL is first proposed by Richards & Hoxey [22]. For fully-developed, steady, incompressible and 2-dimensional ABL flows, the k-ε turbulence model can be simplified to Eqs. (21) and (22) when Eq. (20) is assumed:

$$V = W = \frac{\partial U}{\partial x} = \frac{\partial k}{\partial x} = \frac{\partial \varepsilon}{\partial x} = 0 \tag{20}$$

$$\frac{\partial}{\partial z}\left(\frac{\mu_t}{\sigma_k}\frac{\partial k}{\partial z}\right) + G_k - \rho\varepsilon = 0 \tag{21}$$

$$\frac{\partial}{\partial z}\left(\frac{\mu_t}{\sigma_\varepsilon}\frac{\partial \varepsilon}{\partial z}\right) + C_{\varepsilon 1}G_k\frac{\varepsilon}{k} - \rho C_{\varepsilon 2}\frac{\varepsilon^2}{k} = 0 \tag{22}$$

$$\text{where } G_k = \mu_t\left(\frac{\partial U}{\partial z}\right)^2$$

$$\kappa^2 = \sigma_\varepsilon(C_{\varepsilon 2} - C_{\varepsilon 1})\sqrt{C_\mu} \tag{23}$$

Inlet velocity, k and ε profiles proposed by Richards & Hoxey in 1993 follow the log-law profile as specified from Eqs. (24)-(26). It can subsequently be shown that Eqs. (24)-(26) are the analytical solutions to the $k-\varepsilon$ turbulence model of Eqs. (21) and (22) if Eq. (23) is satisfied. The constants are specified by Launder & Spalding [16], where $C_{\varepsilon 2} = 1.92$, $C_{\varepsilon 1} = 1.44$, $\kappa = 0.42$ and $C_\mu = 0.09$ which results in $\sigma_\varepsilon = 1.225$.

$$U(z) = \frac{u^*_{ABL}}{\kappa}\ln\left(\frac{z + z_0}{z_0}\right) \tag{24}$$

$$k(z) = \frac{(u^*_{ABL})^2}{\sqrt{C_\mu}} \tag{25}$$

$$\varepsilon(z) = \frac{(u^*_{ABL})^3}{\kappa(z + z_0)} \tag{26}$$

The freestream velocity of wind entering the computational domain has a magnitude and direction of 7.93 m/s at a height of 4 m above ground level and $-41°$ respectively. u^*_{ABL} is the frictional velocity of 1.1m/s and roughness length, z_o has a value of 0.19368 m when von Kármán's constant, κ takes a value of 0.42. Concentration is measured in parts per million by volume (ppmv). Standard wall functions with sand-grain roughness modifications following the logarithmic law of the wall where the roughness function $\Delta B = \frac{1}{\kappa}\ln(1 + C_s k_s^+)$ for a fully rough regime (k_s^+>90) are used and k_s^+ is the non-dimensional roughness height. This results in Eq. (27) where $E = 9.793$.

$$u_p = \frac{u^*}{\kappa}\ln\left(\frac{E y^+}{1 + C_s k_s^+}\right) \tag{27}$$

Comparing Eq. (27) with the velocity profiles by Richards & Hoxey, Eq. (24) it is observed that both are similar and hence must be consistent. If profiles proposed by Richards & Hoxey are used and through first-order matching, k_s is given by:

$$k_s = \frac{E z_0 z_p}{C_s(y_0 + y_p)} \tag{28}$$

According to FLUENT [19], the roughness constant C_s is set to a default value of 0.5 which when used with k-ε turbulence models, Nikuradse's original experimental data [23] for flow through a pipe tightly packed with a uniform sand-grain roughness can be replicated. FLUENT subsequently recommended that the range of C_s should lie between 0 and 1 depending on how roughness varies from the uniform sand-grain. However, this range is limited to a specific case of pipe flow as evidenced from lack of a clear guideline on setting C_s for arbitrary types of roughness. Using the default value of C_s in FLUENT results in $k_s \approx 3.8\,m$, based on $z_0 = 0.19368\,m$. Given the multitude of studies [21] [24] [25] which strongly advised that the normal distance from the centre point *P* of the first cell adjacent to the wall z_p to be greater than k_s, it follows that $z_p > 3.8\,m$ and subsequently the height of the first cell adjacent to the wall, $2z_p > 7.6\,m$. This requirement is not practical, given that the height of a container used in this case study is only a mere $2.54\,m$. The result would be a very coarse mesh which would not be able to resolve the flow field accurately. To overcome this, an alternative solution is considered and implemented in this study where the restriction on C_s is relaxed and set equal to E which results in $k_s = z_0$. This condition is enforced in the far-field region of the computational domain

surrounding the near-field region, where the arrays of containers are placed. In the near-field region, k_s is set equal to 0 and C_s equal to 0.5.

Statistical Performance Measures

To quantify the quality of numerical results and their agreement with experimental data, statistical performance measurements are introduced. Following recommendations by Chang et al. [10], the normalized mean square error (NMSE), fractional bias (FB) and the fraction of predictions within a factor of two of observations (FAC2) are used. The definitions of these statistical performance measures are defined below:

$$NMSE = \frac{\overline{(C_o - C_p)^2}}{\overline{C_o}\,\overline{C_p}} \tag{29}$$

$$FB = \frac{(\overline{C_o} - \overline{C_p})}{0.5(\overline{C_o} + \overline{C_p})} \tag{30}$$

$$FAC2 = \frac{N_{0.5 \le \frac{C_p}{C_o} \le 2.0}}{N_{total}} \tag{31}$$

where C_p refers to model predictions while C_o are experimental values. A perfect model would have a value of 1 for FAC2; a value of 0 for FB and NMSE. However, it is well-known that uncertainties will inevitably be present in simulating transport phenomena.

Results & Discussion

CODASC

Grid independence studies were carried out, ensuring the solution no longer changes with mesh density. A mesh size of 14 million cells was found to be adequate. As the flow approaches normal to the street canyon, flow separation results with elements of recirculation inside the canyon. Pollutants released from the ground will be carried by the downward movement of the recirculated flow and deposited on the leeward side. This recirculation is responsible for differences in magnitude of c^+ between both walls as the pollutants gradually accumulate on the leeward side whilst deposits of tracer gas are removed from the windward side. Flow recirculation also traverses in the z-direction, along the length of each building as seen in Fig. 4. Since the entering flow is symmetrical about the z-x plane, the traversing of recirculated flow grows from each end of the street canyon into the z-direction and naturally meets in the middle, which explains why c^+ is highest in the middle of the street canyon. Combining all these elements together will result in concentration distribution in Fig. 5. The streamlines of the airflow in Fig. 4 are colored by velocity magnitude and the contour plot in Fig. 5 is distinguished by normalized concentration c^+.

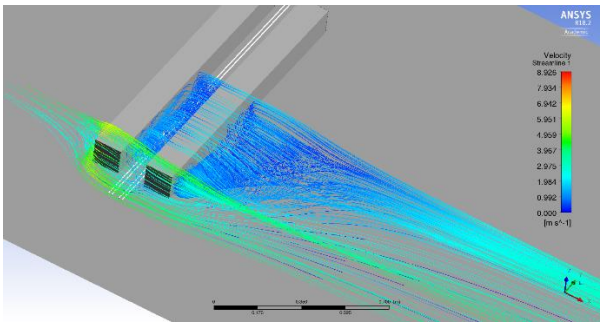

Figure 4. *Velocity (m/s) streamlines obtained from a z-x cutting plane at edge of the model as flow approaches normal to building.*

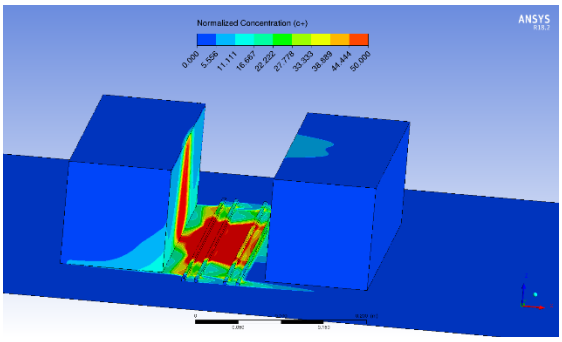

Figure 5. *c^+ distribution in near-field region area of interest.*

Dependence of Sc_t Value on c^+

One of the primary concerns in this study is determining the appropriate value of Sc_t, which is a free parameter, to be used. Given the nature of Sc_t as described earlier, this free parameter can be tuned to artificially reduce or amplify turbulent diffusion or alternatively as it is more commonly done, the value to be used can be obtained from reviews of past studies. The practice of tuning the Sc_t value is ill-advised as evidenced from multiple studies which have warned against it in order to fit the experimental data available [17] [18]. But the use of such tuning practices strengthens the premise that determining the appropriate Sc_t value is problem dependent [17] as flow interacting with different configurations of obstacles have their own turbulent kinetic energy and turbulent diffusion rates. Referring to past studies, Tominaga et al. [17] concluded that dispersion in a street canyon configuration compared to that around a single building will be different, stating that turbulent diffusion is often underestimated in RANS models when applied to single building configuration. With more obstacles present, the increase in turbulent kinetic energy would compensate for that underestimation, hence it is expected that a value greater than 0.3 would provide better prediction results for a street canyon configuration. They went on to conclude that Sc_t values should be considered depending on how dominant turbulent diffusion is in a given flow configuration. But Gromke et al. [12] used RANS simulations of a street canyon for multiple values of Sc_t ranging from 0.2 to 1.0 and found that the value of 0.3 gave the best agreement with experimental results. However, they concluded by recommending a critical review of Sc_t values for future studies on pollutant dispersion in urban environments.

In this case study, RANS simulations were conducted for selected Sc_t values from a range of 0.1 to 0.9 to validate against past studies and to show the effects Sc_t values have on turbulent diffusion. Normalized concentration, c^+ was monitored on both leeward and windward side in the street canyon. On each side, y from 0 to 1.2 were divided into 100 equally spaced discrete points for every z value from 0 to 0.12 in increments of 0.02. Referring to Fig. 6 below, points 1 to 700 represent distribution of c^+ on the leeward side of the street canyon. Similarly, points 701 to 1400 represent distribution of c^+ on the windward side of the street canyon. For example, with reference to Fig. 1, point 1 refers to the red cross marked on the leeward wall, where z = 0 and y = 0. Point 2 is subsequently on z = 0 and y = 0.012 and point 100, denoted by the orange cross is where z = 0 and y = 1.2. Point 101 is continued where $z = 0.02$ and $y = 0$ and so on. Point 701 is on the windward wall, where $z = 0$ and $y = 0$, is denoted by the purple cross. Point 800 is denoted by the black cross which is where $z = 0$ and $y = 1.2$. Point 801, by the same logic, is where $z = 0.02$ and $y = 0$. This accounts for the total of 1400 discrete points to determine the concentration distribution on both leeward and windward walls. By visual

observation, it can be seen that c^+ distribution has been consistently overpredicted on the leeward side and this overprediction increases as the Sc_t value increases in Fig. 6. The same observation applies to the windward side but c^+ is underpredicted when Sc_t has a value of 0.3. c^+ is larger in magnitude on the leeward side and this remains true for all cases simulated.

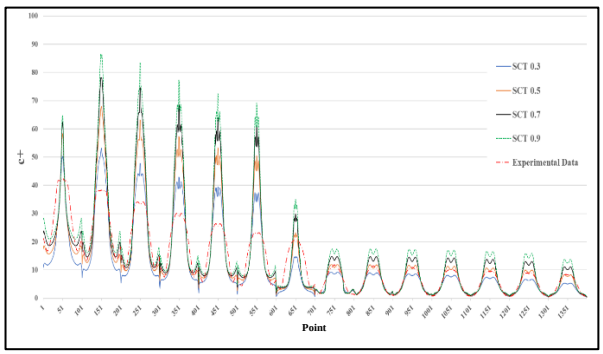

Figure 6. *Plot of c^+ distribution on leeward side followed by windward side in the street canyon.*

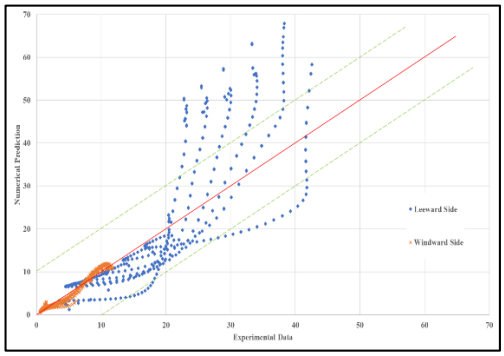

Figure 7. *45° line plot of c^+ distribution when Sc_t = 0.5.*

Fig. 7 shows the deviation between numerical prediction and experimental data for the case when Sc_t= 0.5. The leeward side and windward side are separated for ease of analysis. Data points should ideally lie along the red line and in between the two dotted green lines which provide a band of error on how far these points deviate from experimental measurements. c^+ distribution on the windward wall tend to lie along the 45° line compared to that of the leeward wall, where larger and more frequent deviation is encountered. Due to the extensive number of data points, statistical measures are necessary in order to give a quantitative view of the results which are reflected in Table. 1. Comparing the results, NMSE is lowest for Sc_t 0.3 while FB for Sc_t 0.5 is lowest. Both Sc_t 0.3 and 0.5 share the same value for FAC2 which is close to the ideal value of 1 compared to other Sc_t values. From this analysis, it can be concluded that Sc_t 0.5 is the optimum value for this street canyon case study, simultaneously verifying Tominaga et al. [17] expectations for a Sc_t value greater than 0.3.

Table 1. *Statistical performance measurements for different Sc_t values*

	Sc_t 0.3	Sc_t 0.5	Sc_t 0.7	Sc_t 0.9	Model Perfects
NMSE	0.20	0.31	0.45	0.59	0
FB	0.14	-0.05	-0.17	-0.26	0
FAC2	0.95	0.95	0.92	0.90	1

Contour plots of the leeward wall of the street canyon are presented from Figs. 8 and 9, while contour plots of the windward wall are presented from Figs. 10 and 11. These are positioned on the $z-y$ plane. The contour plots are all symmetrical about the z-axis, which serves as a form of validation between model and physical reality. c^+ at the two ends of both leeward and windward walls is relatively lower due to more dominant convection forces from vortices generated from the interaction between the flow and the street canyon.

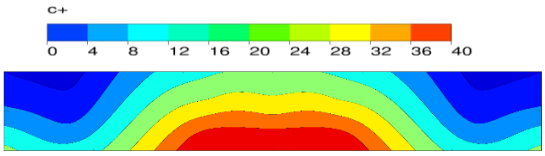

Figure 8. *c^+ distribution of experimental result for leeward wall.*

Figure 9. *c^+ distribution of numerical result on leeward wall when Sc_t = 0.5.*

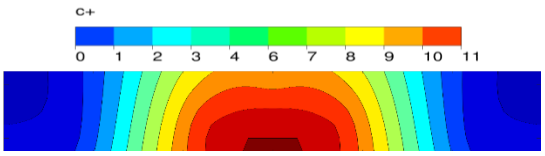

Figure 10. *c^+ distribution of experimental result for windward wall.*

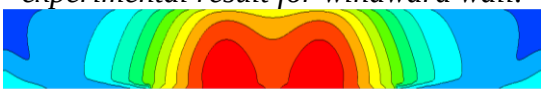

Figure 11. *c^+ distribution of numerical result on windward wall when Sc_t = 0.5.*

Comparison Between Passive Scalar and Multi-Species Transport Models

For the multi-species model, a Sc_t value of 0.5 is used based on earlier findings from the passive scalar model. As seen in Table 2, the passive scalar transport model outperforms the multi-species model in every statistical benchmark, which is unexpected as it is initially believed that the multi-species model will instead outperform the passive scalar transport model since the pollutant considered is denser than air. Density of the flow field is expected to change due to changes in the mass fraction of pollutant in air because of the coupling of momentum equations with the continuity equation. Similarly, Fig. 12 to Fig. 15 show the respective contour plots.

Table 2. *CODASC: Comparison of passive scalar and multi-species transport model through statistical performance measures.*

	Passive Scalar Transport Model	Multi-Species Transport Model	Model Perfects
NMSE	0.31	1.99	0
FB	-0.05	-0.48	0
FAC2	0.95	0.87	1

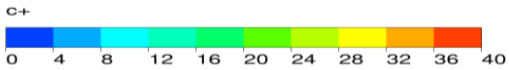

Figure 12. *CODASC: c^+ distribution on the leeward wall (Passive Scalar Model).*

Figure 13. *CODASC: c^+ distribution on the leeward wall (Multi-Species Model).*

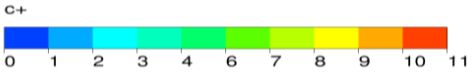

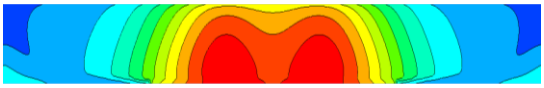

Figure 14. *CODASC: c^+ distribution on the windward wall (Passive Scalar Model).*

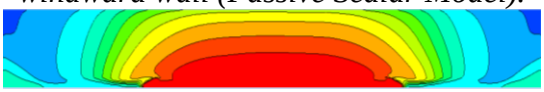

Figure 15. *CODASC: c^+ distribution on the windward wall (Multi-Species Model).*

Mock Urban Setting Test (MUST)

In order to determine if some form of homogeneity has been achieved with the current parameters set, the profiles of velocity in the y-direction, k and ε are monitored. Referring to Fig. 16, profiles at y_1 and y_2 are tracked as flow progresses from the far-field region to the near-field region, especially since grid density changes are involved. Fig. 17 shows the y-velocity profiles with the analytical profile, the k and ε profiles with their respective analytical profiles as z increases. The velocity profiles in Fig. 17 reflects a relatively good agreement between the analytical profile and y_1 and y_2 save for some deviations on the order of approximately 0.1. k profiles, on the other hand, show an increasing deviation from the

analytical profile with increasing z. The profile of y_1 deviate from y_2 near the ground and generally show an underprediction of turbulent kinetic energy. According to Richards and Norris [26], the local maximum in turbulent kinetic energy k at y_2 is due to an inconsistency in the discretization of the production term P_k instead of the turbulence model itself. The ε profiles show no differences between the analytical profile, y_1 and y_2 except for the near-ground region.

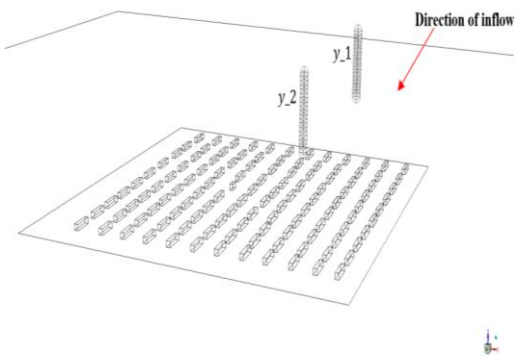

Figure 16. *Locations in the MUST case where v, k and ε profiles are taken and monitored from.*

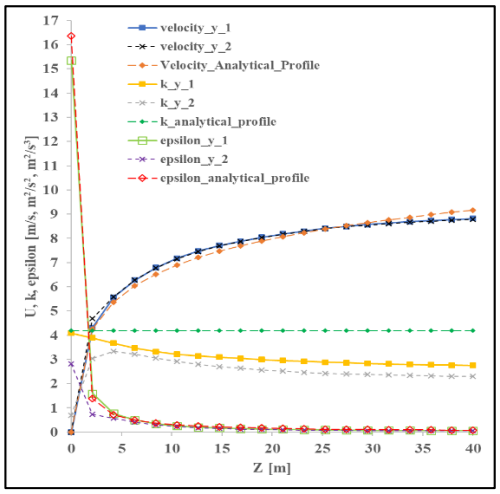

Figure 17. *Plot of Z against mean velocity, k and ε profiles for MUST case.*

As the incoming flow approaches the near-field region, the presence of containers forces the flow to be diverted with recirculation around each individual container and is deflected upwards. Complexity surrounding this flow configuration is significantly greater than the street canyon case given that the flow enters at an inclined angle. The streamlines of the fluid flow are shown in Fig. 18, where it is colored by velocity magnitude. According to the coloration of the streamlines, it is observed that a slight acceleration of the flow persists despite enforcing the horizontal homogeneity condition when flow transits from the far-field to near-field region. It is also noted that behind each container, the velocity of streamlines drops to almost zero.

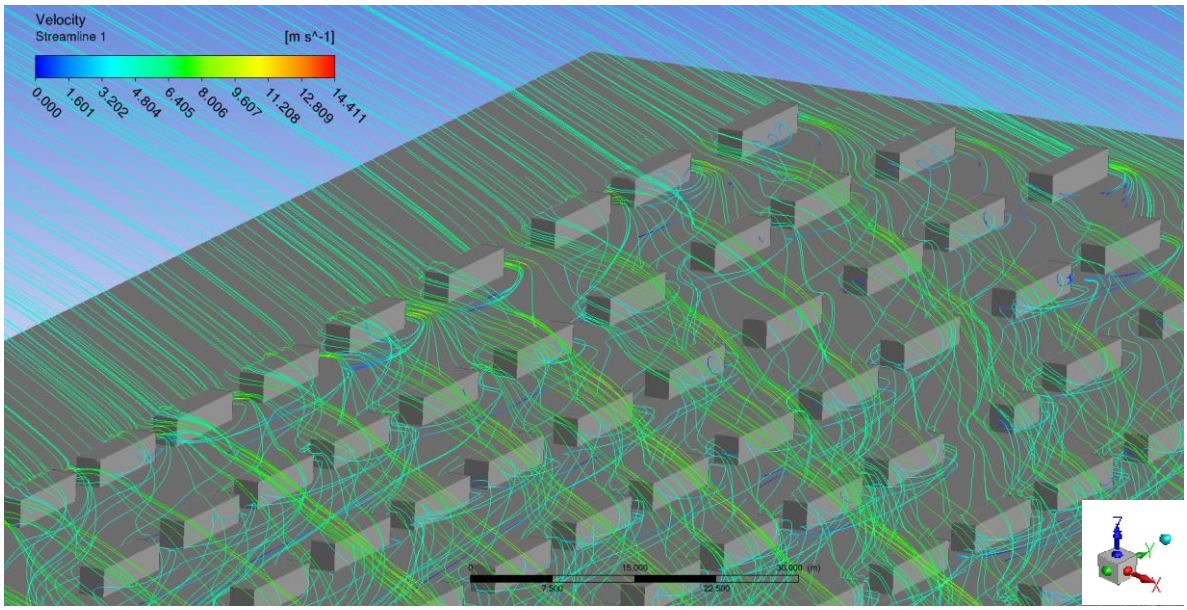

Figure 18. *Velocity streamlines of flow entering the near-field domain at a $-41°$ angle of the MUST case.*

Dependence of Sc_t Value on c^+

Given the flow configuration in MUST varies significantly from the street canyon model due to different geometries, it is expected that the optimal Sc_t would be different. Experimental data is readily available from on-site measurements which adds ease to validation. Based on visual observations of Fig. 19, the most noticeable trend is that numerical results consistently underpredict c^+. Using statistical performance measures in Table 3., NMSE appears to be lowest for Sc_t 1.5, while FB is lowest for Sc_t 2. Both Sc_t 1.5 and 2 share the same FAC2 of 0.47. Comparing NMSE and FB of Sc_t 1.5 and Sc_t 2 leads to conflicting results and can be concluded that there are limited differences between these two Sc_t values. However, a conclusion can be drawn in that Sc_t values of 1.5 and higher will result in better agreement with experimental data. Fig. 20 show the contour plot of Sc_t value equal to 1.5 which ranges from 0 $ppmv$ to 6 $ppmv$. The inlet flow is at an angle of $-41°$, which is stated to be the mean angle based on data obtained by field experiments [14].

Table 3. *Statistical performance measurements of various Sc_t values for the MUST case.*

	Sc_t 0.5	Sc_t 0.7	Sc_t 0.9	Sc_t 1.5	Sc_t 2	Model Perfects
NMSE	1.68	1.08	0.78	0.55	0.59	0
FB	0.95	0.81	0.70	0.49	0.39	0
FAC2	0.03	0.21	0.35	0.47	0.47	1

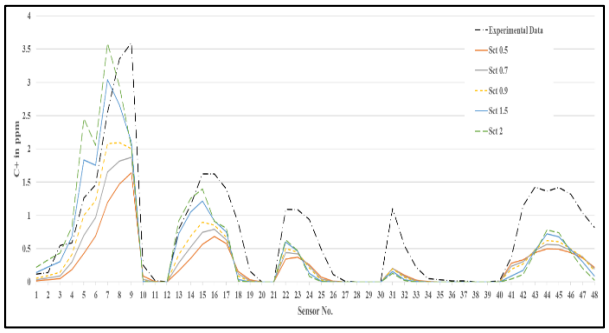

Figure 19. *Plot of numerical c^+ data from 48 sensors placed at various locations with increasing Sc_t values in the MUST case.*

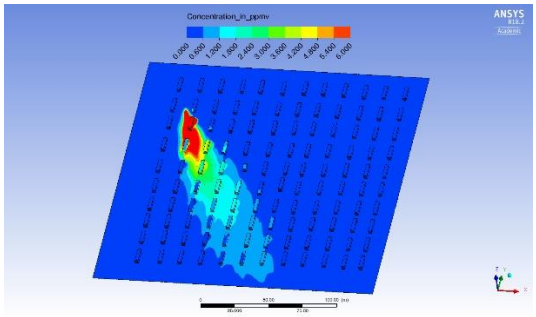

Figure 20. *c^+ distribution with Sc_t = 1.5 for MUST case.*

Comparison Between Passive Scalar and Multi-Species Transport Models

Next, a comparison of accuracy in predicting c^+ between the passive scalar transport model and multi-species model is made. Sc_t value of 1.5 is taken for both cases. From Fig. 21, the multi-species model provides better agreement with experimental results compared to the passive scalar model. Significant underprediction of numerical results continue to persist, with increasing deviation away from the source release. A similar conclusion is also reached by examining the statistical performance measures in Table 4. NMSE and FB indicate that the multi-species model gave results closer to perfect model values than the passive scalar model did while both models hold the same values for FAC2 of 0.47. Fig. 22 and Fig. 23 show the degree of dispersion with different methodologies used.

Table 4. *Comparison of statistical performance measures of passive scalar and multi-species transport model against the model perfects.*

	Passive Scalar	Multi-Species	Model Perfects
NMSE	0.55	0.45	0
FB	0.49	0.31	0
FAC2	0.47	0.47	1

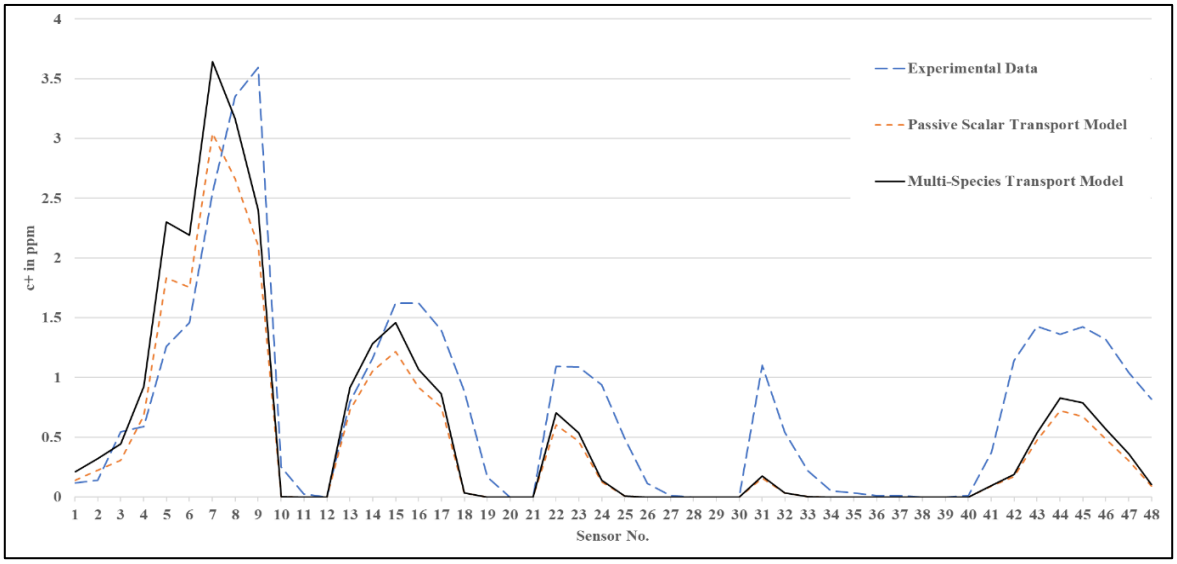

Figure 21. *Plot of numerical c^+ data for passive scalar and multi-species transport model with Sc_t = 1.5 of 48 sensors placed at various locations for MUST case.*

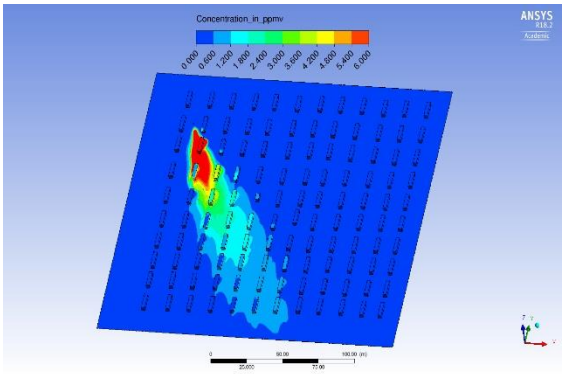

Figure 22. *c^+ distribution of passive scalar transport model in MUST case with the mean inflow angle of $-41°$.*

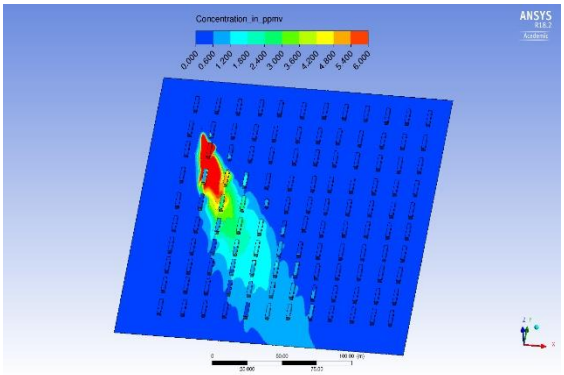

Figure 23. *c^+ distribution of multi-species transport model in MUST case with the mean inflow angle of $-41°$.*

Variation of Inflow Angles

In an attempt to investigate further the discrepancy in concentration of pollutant far from the source release, the inlet boundary conditions are examined in further detail. A standard deviation of 9.5° in the instantaneous wind direction is provided as reflected by Yee and Biltoft [27]. Likewise, an additional point mentioned by Nadir et al. [13] was the standard deviation of the inlet flow angle of $-41°$ but this was overlooked as a potential source of error in his paper. This is considered in the present study and following the deviation of $-9.5°$, two separate additional cases with the inflow angle of $-31.5°$ and $-50.5°$ were simulated. In Fig. 24, the inflow at an angle of $-31.5°$ clockwise from the positive x-axis resulted in better agreement compared to the case with an angle $-41°$ clockwise from the positive x-aixs. Underprediction still occurs, albeit at a lower occurrence when inflow angle deviates to $-31.5°$ and it is mostly limited to the tower of sensors numbered 40 to 48. This is further evidenced in Table 5., where the case with inflow angle of $-31.5°$ performed significantly better on every statistical performance measure. When inflow is angled at $-50.5°$, the opposite occurs in that the model performed worse. These cases are simulated using a Sc_t value of 1.5. This was repeated using the multi-species transport model and a similar conclusion can be drawn. The above attempts

in carrying out studies involving the change in inflow angles conclusively show a source of error originating from comparing field experiments with numerical studies. This error is expected and inevitable when carrying out full-scale outdoor experiments.

Table 5. *Statistical performance measures against model perfects for varying inflow angles with the passive scalar transport model in MUST case.*

	$-41°$	$-31.5°$	$-50.5°$	**Model Perfects**
NMSE	0.55	0.21	2.31	0
FB	0.49	0.28	0.76	0
FAC2	0.47	0.65	0.18	1

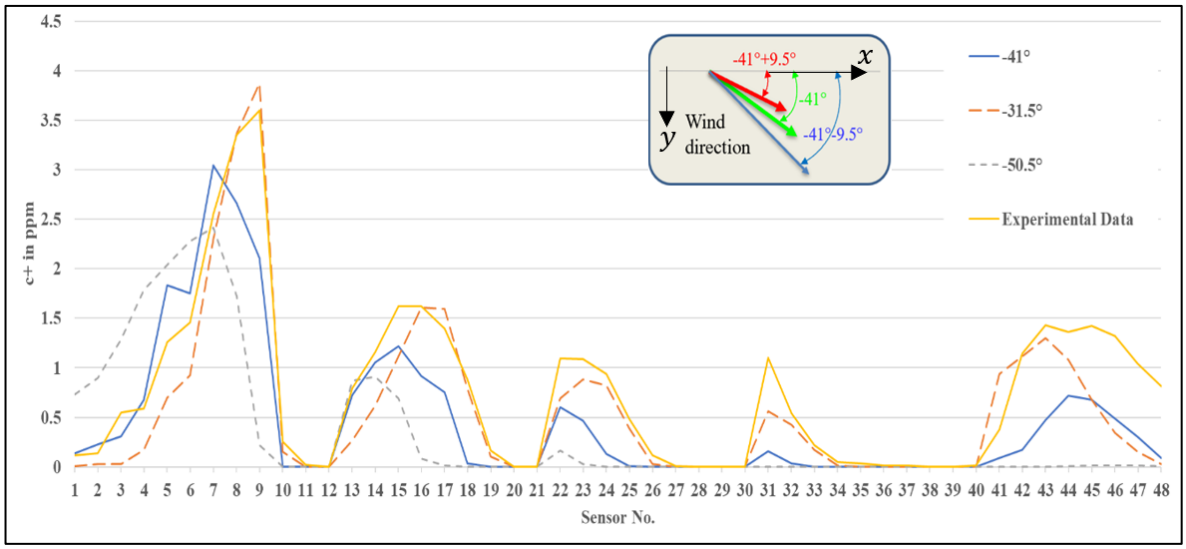

Figure 24. *Plot illustrating the numerical c^+ data from 48 sensors placed at various locations in the MUST case, with different inflow angles using the passive scalar transport model compared against experimental data.*

Conclusion

A comparison between two different transport methodologies was carried out through their respective validation against two test cases; the CODASC model and MUST. The CODASC experiment was carried out under controlled conditions in a wind tunnel whereas MUST is a full-scale outdoor experiment, taking into account effects of the atmospheric boundary layer. Results from CODASC study proved that the passive scalar transport model outperformed the multi-species transport model and the opposite for MUST. In reality, it is expected that the multi-species model will provide better accuracy since density changes caused by species compositions in the flow field are taken into account. Furthermore, pollutants heavier than air in terms of molecular weight were used in simulating transport phenomena for both cases, allowing the physical dispersion process to be more accurately represented.

Hence, it is concluded that since the multi-species transport model did not provide significant improvement over the passive scalar transport model in general, the multi-species model should be dismissed until further investigations can prove its worth. Furthermore, for engineering applications where computational efficiency is a major component in determining which methodology to use, it should be noted that the passive scalar transport model is much more efficient compared to the multi-species transport model. Time taken for a simulation using the passive scalar transport model can be up to three times shorter compared to using the multi-species model.

For CODASC case study, limited information on how the four lines of tracer source release were modeled in both wind tunnel experiments and numerical studies that it is believed the results from this present study could only be justified with the assumption of a dilute source. For MUST, given that it is a full-scale outdoor experiment, it would be unrealistic to expect the magnitude and direction of the inlet wind flow be maintained throughout the course of the experiment, though it is an assumption necessary for numerical studies lest the level of complexity be increased. Through investigations on the variations of inflow angles, it suggests that the inflow angle did not remain constant at $-41°$ during field experiments. Differences in configuration of obstacles in both cases could play a major role in prohibiting the full realisation of benefits in utilising the multi-species transport model. Efforts to remove the turbulent Schmidt number, Sc_t should be a priority in reducing ambiguity in dispersion studies using CFD.

References

[1] https://www.independent.co.uk/news/world/asia/fukushima-nuclear-disaster-radiation-lethal-levels-leak-japan-tsunami-tokyo-electric-power-company-a8190981.html (Date of last access: 10/4/2019)

[2] https://www.nst.com.my/world/2018/11/436113/gas-leak-caused-deadly-blast-china-olympic-city (Date of last access: 10/4/2019)

[3] Á. Leelőssy, F. Molnár, F. Izsák, Á. Havasi, I. Lagzi, and R. Mészáros, "Dispersion modeling of air pollutants in the atmosphere: a review," *Central European Journal of Geosciences*, vol. 6, no. 3, pp. 257–278, Sep. 2014.

[4] Lateb, M., et al. "On the Use of Numerical Modelling for near-Field Pollutant Dispersion in Urban Environments −A Review." *Environmental Pollution*, vol. 208, 2016, pp. 271–283., doi: 10.1016/j.envpol.2015.07.039.

[5] M. Mohan, "Analysis of various schemes for the estimation of atmospheric stability classification," *Atmospheric Environment*, vol. 32, no. 21, pp. 3775–3781, 1998.

[6] Adel A. Abdel-Rahman, "On the Atmospheric Dispersion and Gaussian Plume Model," in *2nd International Conference on Waste Management, Water Pollution, Air Pollution, Indoor Climate (WWAI'08)*, Corfu, 2008.

[7] R. MacDonald, "Theory and Objectives of Air Dispersion Modelling", Modelling Air Emissions for Compliance MME 474A Wind Engineering, Dec. 2003.

[8] Y. Tominaga and T. Stathopoulos, "CFD simulation of near-field pollutant dispersion in the urban environment: A review of current modeling techniques," *Atmospheric Environment*, vol. 79, pp. 716–730, 2013.

[9] Y. Tominaga and T. Stathopoulos, "Ten questions concerning modeling of near-field pollutant dispersion in the built environment," *Building and Environment*, vol. 105, pp. 390–402, 2016.

[10] J. C. Chang and S. R. Hanna, "Air quality model performance evaluation," *Meteorology and Atmospheric Physics*, vol. 87, no. 1-3, pp. 167–196, Jun. 2004.

[11] C. B. Gromke, "CODASC: a database for the validation of street canyon dispersion models," *In Proceedings of the 15th International Conference on Harmonisation within Atmospheric Dispersion Modelling for Regulatory Purposes (HARMO)*, May 2013.

[12] C. Gromke and B. Ruck, "Dispersion study in a street canyon with tree planting by means of wind tunnel and numerical investigations – Evaluation of CFD data with experimental data," *Atmospheric Environment*, vol. 42, no. 37, pp. 8640–8650, Dec. 2008.

[13] N. Bekka, P. Kumar, A. A. Feiz, S. Singh, M. Sellam, E. Barbosa, P. Ngae, G. Turbelin, A. Chpoun, "A CFD MODELING APPROACH FOR A CONTAMINANT RELEASED IN A CITY", in *17th International Conference on Harmonisation within Atmospheric Dispersion Modelling for Regulatory Purposes*, Budapest, Hungary, 9-12 May 2016.

[14] C. A. Biltoft, "Customer Report for Mock Urban Setting Test," *DPG Document No. WDTCFR- 01-121, West Desert Test Center, U. S. Army Dugway Proving Ground, Dugway, Utah*, 58 pp., 2001

[15] Y. Tominaga and T. Stathopoulos, "CFD simulations of near-field pollutant dispersion with different plume buoyancies," *Building and Environment*, vol. 131, pp. 128–139, 2018.

[16] B. E. Launder and D. B. Spalding, "The numerical computation of turbulent flows," *Computer Methods in Applied Mechanics and Engineering*, vol. 3, no. 2, pp. 269–289, 1974.

[17] Y. Tominaga and T. Stathopoulos, "Turbulent Schmidt numbers for CFD analysis with various types of flowfield," *Atmospheric Environment*, vol. 41, no. 37, pp. 8091–8099, 2007.

[18] C. Gualtieri, A. Angeloudis, F. Bombardelli, S. Jha, and T. Stoesser, "On the Values for the Turbulent Schmidt Number in Environmental Flows," *Fluids*, vol. 2, no. 2, p. 17, 2017.

[19] ANSYS® FLUENT Release 18.2 Theory Guide, August 2017.

[20] https://www.windforschung.de/CODASC.htm (Date of last access: 10/4/2019)

[21] B. Blocken, T. Stathopoulos, and J. Carmeliet, "CFD simulation of the atmospheric boundary layer: wall function problems," *Atmospheric Environment*, vol. 41, no. 2, pp. 238–252, 2007.

[22] P. Richards and R. Hoxey, "Appropriate boundary conditions for computational wind engineering models using the k-ε turbulence model," *Journal of Wind Engineering and Industrial Aerodynamics*, vol. 46-47, pp. 145–153, 1993.

[23] J. Nikuradse, "Laws of Flow in Rough Pipes," *VDI Forschungsheft*, July/August 1933.

[24] Parente, Alessandro, "CFD boundary conditions, turbulence models and dispersion study for flows around obstacles," 2013.

[25] B. Blocken, J. Carmeliet, T. Stathopoulos, "CFD evaluation of wind speed conditions in passages between parallel buildings—effect of wall-function roughness modifications for the atmospheric boundary layer flow" *Journal of Wind Engineering and Industrial Aerodynamics*, vol. 95, no. 9–11, pp. 941–962, 2007, https://doi.org/10.1016/j.jweia.2007.01.013.

[26] P. J. Richards and S. E. Norris, "Appropriate boundary conditions for computational wind engineering models revisited," *Journal of Wind Engineering and Industrial Aerodynamics*, vol. 99, no. 4, pp. 257–266, 2011.

[27] E. Yee and C. A. Biltoft, "Concentration Fluctuation Measurements in a Plume Dispersing Through a Regular Array of Obstacles," *Boundary-Layer Meteorology*, vol. 111, no. 3, pp. 363–415, 2004.